Journal of Materials Chemistry B

Accepted Manuscript

ROYAL SOCIETY OF CHEMISTRY

www.rsc.org/materialsB

Journal Name

ARTICLE

Three dimensional Pt nanodendrites/graphene/MnO_2 nanoflowers modified electrode for sensitive and selective detection of dopamine

Received 00th January 20xx,
Accepted 00th January 20xx

DOI: 10.1039/x0xx00000x

www.rsc.org/

Beibei Yang[a], JinWang[a], Duan Bin[a], Mingshan Zhu*[b], Ping Yang[a], Yukou Du*[a]

An electrochemical sensor using novel three dimensional (3D) ternary Pt nanodendrites/reduce graphene oxide/MnO_2 nanoflowers (Pt/RGO/MnO_2) modified glassy carbon electrode was proposed for the selective and sensitive determination of dopamine (DA) in the presence of ascorbic acid (AA) and uric acid (UA). Cyclic voltammetry (CV) and differential pulse voltammetry (DPV) were used to evaluate electrochemical behaviors of DA on the as-prepared electrode. The oxidation peak current of DA is linearly proportional to its concentration in the range from 1.5-215.56 μM, with a detection limit of 0.1 μM (at S/N=3). Compared to bare RGO, Pt nanodendrites/RGO and MnO_2 nanoflowers modified electrodes, the 3D hierarchical ternary Pt/RGO/MnO_2 composites displayed the highest electrocatalytic activity of the selective detection of DA. Moreover, the 3D Pt/RGO/MnO_2 modified electrode can be reused with no obvious deterioration in the electrocatalytic performance. This work paves the way for developing a novel 3D nanostructure and offers new opportunities for improving the performance of electrochemical sensors with excellent sensitivity, repeatability and anti-interference.

1. Introduction

Dopamine (DA), as an excitatory neurotransmitter, plays an important role in various physiological actions such as behavior, mood and movement, which means an accurate monitoring of the concentration of DA is essential for nerve physiology study and diagnosis.[1-5] However, in the functions of central nervous system, the basal DA concentration is very low (0.01–1 μM).[5] To date, various advanced analytical methods have been developed, while the direct electrochemical technique for DA analysis, as a rapid detection, simplicity, sensitive, cost and time effectiveness, is drawing increasing attention.[1-5] It is notable that a major problem in its determination is the coexisting compounds such as uric acid (UA) and ascorbic acid (AA), which can cause great interference due to the concentration is much higher than DA and the similar oxidation potential is close to that of DA. Moreover, the oxidation product of AA or UA on electrode surface will result in poor selectivity and reproducibility.[3,5]

To resolve these problems, one strategy is to use various noble metal nanostructures in the construction of the working electrode to enhance the sensitivity and repeatability and anti-interference for the detection of DA.[6-9] Dendritic platinum nano-architectures, with richly branched structures, have attracted significant attention in recent years due to their fascinating properties and potential applications in catalysis, electronics and chemical sensors.[9-13] This stems from their large surface-to-volume ratio, abundant edges and corner atoms, high surface roughness, *etc.* Towards this aim, great efforts have been devoted to synthesize three-dimensional (3D) dendritic nanostructures, where a template or surfactant, such as Pluronic F127, polyvinyl pyrrolidone (PVP) was usually required in the growth processes.[10-12] Recently, graphene-based nanomaterial as a novel 2D support material for the synthesis of dendritic noble metal nanocomposites have received broad interests because of graphene-based material was used not only as a support for the deposition of noble metal structures but also as functional promoter.[13-16] This is owing to graphene possesses large specific surface area, unique electronic properties, unique physicochemical properties, high chemical and thermal stability.[17,18]

On another front, as a potentially excellent electrode material in electrochemical application such as supercapacitors, nanostructure MnO_2 has attracted particularly attention owing to their peculiar properties including high catalytic activity, good chemical stability, low-cost, environmental friendliness and high energy density.[19-21] In this regard, great efforts have been paid on the extension of nanostructure MnO_2 for other applications such as catalysis, sensors and so on.[22-26] For instance, Xu et al have prepared the co-catalysis of hemin/G-quadruplex platinum nanoparticles and flower-like MnO_2 nanosphere functionalized multi-walled carbon nanotubes electrode for the sensitive detection of thrombin.[27] Zhang et al have provided an easy approach to synthesize graphene

nanosheets attached to spiky MnO_2 nanospheres which was applied in the detection of carcinoembryonic antigen.[28] Considering the importance of detection of DA with high sensitive and selective, and attractive merits of combining dendritic Pt nanostructures, graphene and MnO_2 nanostructures, an investigation on these ternary complexes for the electrochemical determination of DA might be meaningful. Herein, we developed a new three dimensional (3D) hierarchical ternary composite including Pt nanodendrites/reduce graphene oxide/MnO_2 nanoflowers (Pt/RGO/MnO_2) modified glassy carbon electrode for the selective and sensitive determination of DA in the presence of AA and UA. The 3D hierarchical ternary electrode displays significant improvement of electrocatalytic performance for selective detection of DA compared to bare graphene, Pt nanodendrites/RGO and MnO_2 nanoflowers modified electrodes. The 3D Pt/RGO/MnO_2 composite displayed the highest electrocatalytic activity of selective detection of dopamine. This work might open up new opportunities for developing novel 3D electrochemical sensors with excellent sensitivity and reproducibility.

2. Experimental

2.1 Materials and reagents

Graphite powder, disodium hydrogen phosphate (Na_2HPO_4), sodium dihydrogen phosphate (NaH_2PO_4), potassium permanganate ($KMnO_4$), manganese sulfate ($MnSO_4$), ethanol and $H_2PtCl_6 \cdot 6H_2O$ were purchased from Sinopharm Chemicals Reagent Co., Ltd. Ascorbic acid (AA), uric acid (UA) and dopamine (DA) were obtained from Acros Organics. All reactants were used as received without further purification. Phosphate buffer solution (PBS, 0.1 mol L^{-1}, pH 7.0) was prepared from NaH_2PO_4 and Na_2HPO_4. Double distilled water was used throughout the experimental process.

2.2 Apparatus

The morphology and structure of the obtained electrode were analyzed by transmission electron microscopy (TEM) and high-resolution TEM (HRTEM) measurements on a Tecnai G220 electron microscope operating at an accelerating voltage of 200 kV. Scanning electron microscope (SEM) and energy dispersive X-ray analyzer (EDX) were conducted with the S-4700 system (Hitachi High Technologies Corporation, Japan). X-ray diffraction (XRD) analysis was carried out on a PANalytical X'Pert PRO MRD X-ray diffractometer with Cu Kα radiation (λ = 1.54056 Å) operated at 40 kV and 30 mA. Raman spectra were obtained on a Renishaw Invia Plus Raman microscope using a 633 nm argon ion laser. X-Ray photoelectron spectroscopy (XPS) was performed on an ESCALab220i-XL electron spectrometer from VG Scientific using 300 W Al Kα radiation. The electrochemical experiments were carried out in a CHI 650D electrochemical station (Shanghai Chenhua Instrumental Co., Ltd., China) with a conventional three-electrode system. The glassy carbon electrode (GCE) with a diameter of 3 mm and its modified electrode were used as working electrodes. A Pt wire and a saturated calomel electrode (SCE) acted as the counter and reference electrodes, respectively.

2.3 Synthesis of dendritic Pt nanostructures modified RGO nanosheets

Firstly, GO was synthesized from graphite powder according to the modified Hummers method. 20 mg GO was dispersed into 20 mL H_2O by ultrasonication for at least 1 h, followed by the addition of 6 mL $H_2PtCl_6 \cdot 6H_2O$ (7.2 mg mL^{-1}) aqueous solution into the brown GO ink. Subsequently, 20 mL of ethanol was added into the mixture. The pH of the mixture was adjusted to 10.5 with the aid of 0.1 M NaOH aqueous solution. Afterwards, the mixture was refluxed in an oil bath at 90 °C for 4 h under constant stirring to ensure the complete reduction of the GO and metal salt. Finally, the sample was collected after thoroughly rinsing with deionized water, and dispersed in 40 mL water as stock solutions of 0.5 mg mL^{-1} via 10 minutes sonication. The bare RGO was obtained by same condition without $H_2PtCl_6 \cdot 6H_2O$ aqueous solution.

2.4 Synthesis of MnO_2 nanoflowers, ternary Pt nanodendrites/ reduced graphene oxide/MnO_2 nanoflowers

Firstly, 1.51 g $MnSO_4$ and 3.95 g $KMnO_4$ were initially dissolved in 50 mL water by ultrasonication for 1 h. Then, the mixture was transferred into a 100 mL Teflon-lined autoclave and subsequently heated at 160 °C for 24 h. When it cooled down to room temperature naturally, the obtained MnO_2 nanoflowers were harvested by centrifugation and washed with water, and were finally vacuum-dried at 80 °C over a night. The 3D ternary Pt/RGO/MnO_2 nanocomposite was obtained via mixing the as-prepared Pt/RGO and the MnO_2 nanoflowers by van der Waals interactions under ultrasonication. Detailly, 2.5 mg as-synthesized MnO_2 with 200 µL Nafion solution (5 wt%) was dispersed into 5 mL as-prepared Pt/RGO (0.5 mg mL^{-1}) under ultrasonication for 60 minutes. The sediment were collected by centrifugation and washed thoroughly with water, resulting in ternary Pt/RGO/MnO_2 nanocomposites.

2.5 Preparation of Pt/RGO/MnO_2, RGO, Pt/RGO and MnO_2 nanoflowers modified electrode

The Pt/RGO/MnO_2, RGO, Pt/RGO and MnO_2 nanoflowers modified glassy carbon electrodes (GCEs) were prepared: Firstly, the Pt/RGO/MnO_2, RGO, Pt/RGO and MnO_2 nanoflowers were dispersed in water under ultrasonication for forming 0.5 mg mL^{-1} aqueous dispersion. Then, 10 µL of the as-prepared dispersions (0.5 mg mL^{-1}) were spread on the GCE surface and dried at 30°C in vacuum oven, resulting in Pt/RGO/MnO_2, RGO, Pt/RGO and MnO_2 nanoflowers modified GCEs.

3. Results and discussion

3.1 Characterization of 3D hierarchical ternary Pt/RGO/MnO_2 nanocomposite

Firstly, our Pt nanodendrites hybridized with RGO nanosheets could be obtained easily by wet-chemical method. The GO worked as both inductor and stabilizer during the synthetic

process. The different magnifications morphologies of produced nanostructures were characterized by transmission electron microscopy (TEM), as shown in Fig. 1. The low-magnification TEM images (Fig. 1A and 1B) show that the Pt nanodendrites are uniformly distributed on the wrinkled RGO surface. It can be seen that each of the as-synthesized Pt nanodendrite was composed of many small arms of Pt nanoparticles. The average overall size of these Pt nanodendrites was found to be *ca.* 15 nm and the average diameter of each branch of Pt nanodendrites is *ca.* 2 nm. The high-resolution TEM (HRTEM) images (Fig. 1C and 1D) indicate that the arms of Pt nanodendrites present a single-crystalline structure. The interplanar spacing is 0.23 nm, which agrees well with the (111) lattice spacing of face-centered-cubic Pt.[12,26]

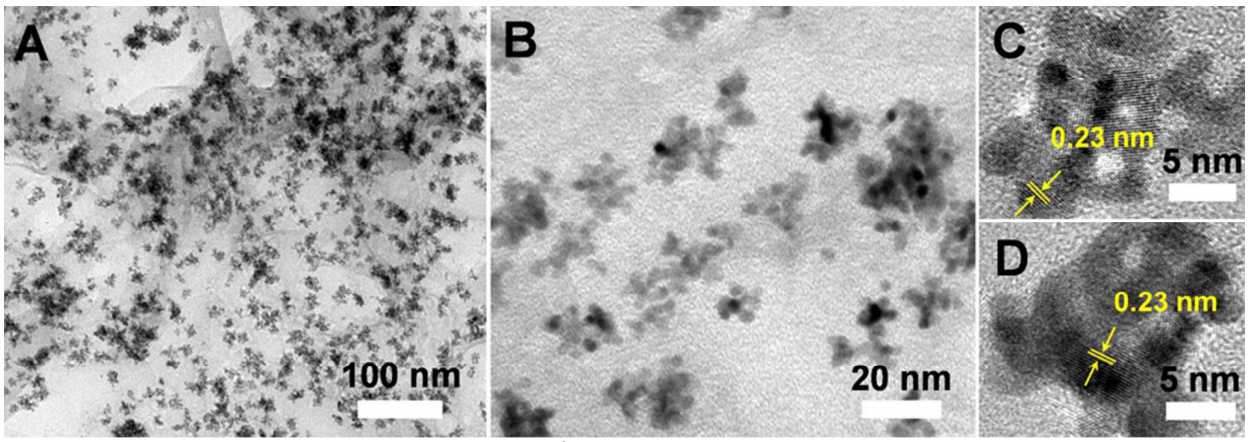

Fig. 1. TEM (A and B) and HRTEM (C and D) images of dendritic Pt/RGO nanostructures.

The platelike MnO_2 nanoflowers were facile synthesized by the hydrothermal method. The SEM images of the as-prepared MnO_2 (Fig. 2A and 2B) solidly demonstrate the as-prepared α-MnO_2 possesses flower-like sheets. The total size of the MnO_2 nanoflower is *ca.* 400 nm. The TEM and magnified TEM images (Fig. 2C and 2D) further visually confirm the formation of 3D platelike MnO_2 nanoflowers. The fine structure of the as-synthesized MnO_2 nanoflowers is thin sheet-like structure. Additionally, the HRTEM image of MnO_2 structure indicates the lattice fringes with interplanar distances of approximately 0.69 nm shown in Fig. 2E, which corresponds to the (110) crystal plane of the α-MnO_2 (JCPDS, file no. 44-0141).[19]

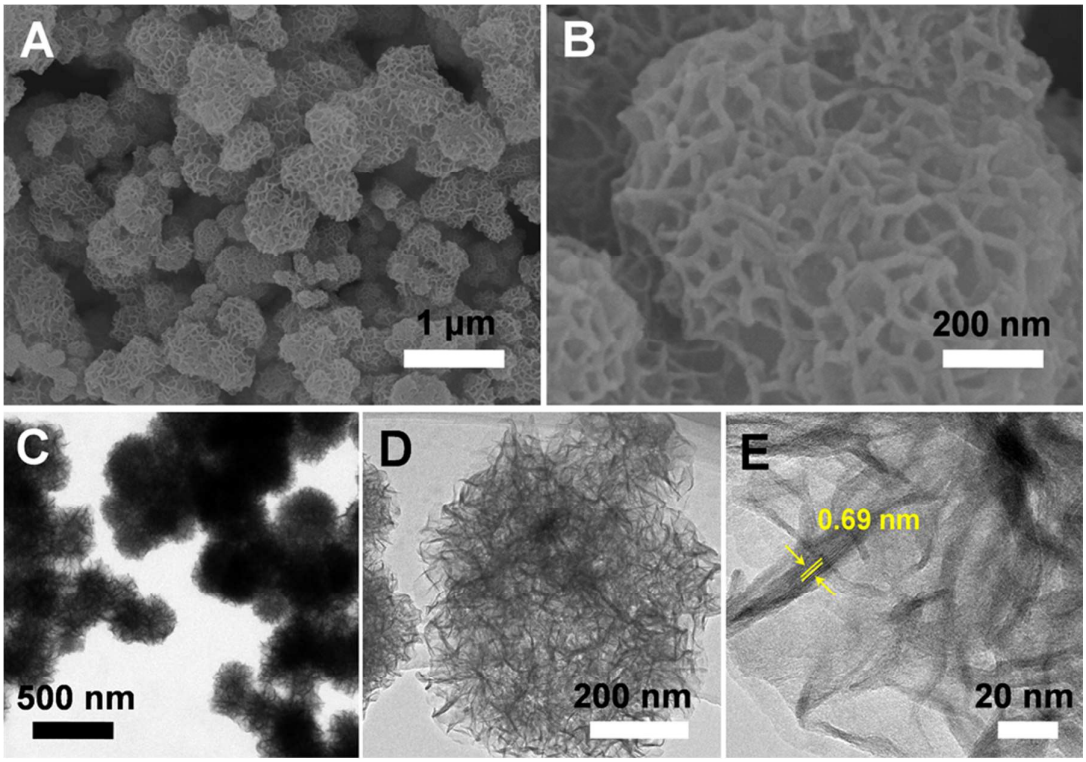

Fig. 2. SEM (A and B), TEM (C and D) and HRTEM (E) images of MnO_2 nanoflowers.

The 3D ternary Pt/RGO/MnO_2 nanocomposite was obtained by mixing the as-prepared Pt/RGO and the MnO_2 nanoflowers under ultrasonication. The platelike MnO_2 sheets will assemble on the surface of dendritic Pt/RGO nanostructures by van der Waals interactions.[20] As shown in Fig. 3A and 3B, the SEM images indicated that the MnO_2 nanoflowers were enwrapped with the dendritic Pt/RGO nanocomposites. The fine structure of this ternary composite was further examined by TEM image. Fig. 3C and 3D show the dendritic Pt/RGO nanocomposites were dispersed on the surface of platelike MnO_2 sheets. The compositions of the 3D Pt/RGO/MnO_2 composites were determined by EDX analysis and element mapping, as shown in Fig. S1. The elements of C, O, Mn and Pt were homogeneously distributed throughout the 3D Pt/RGO/MnO_2 composites, suggesting the presence of Pt, RGO, MnO_2 species in as-prepared samples.

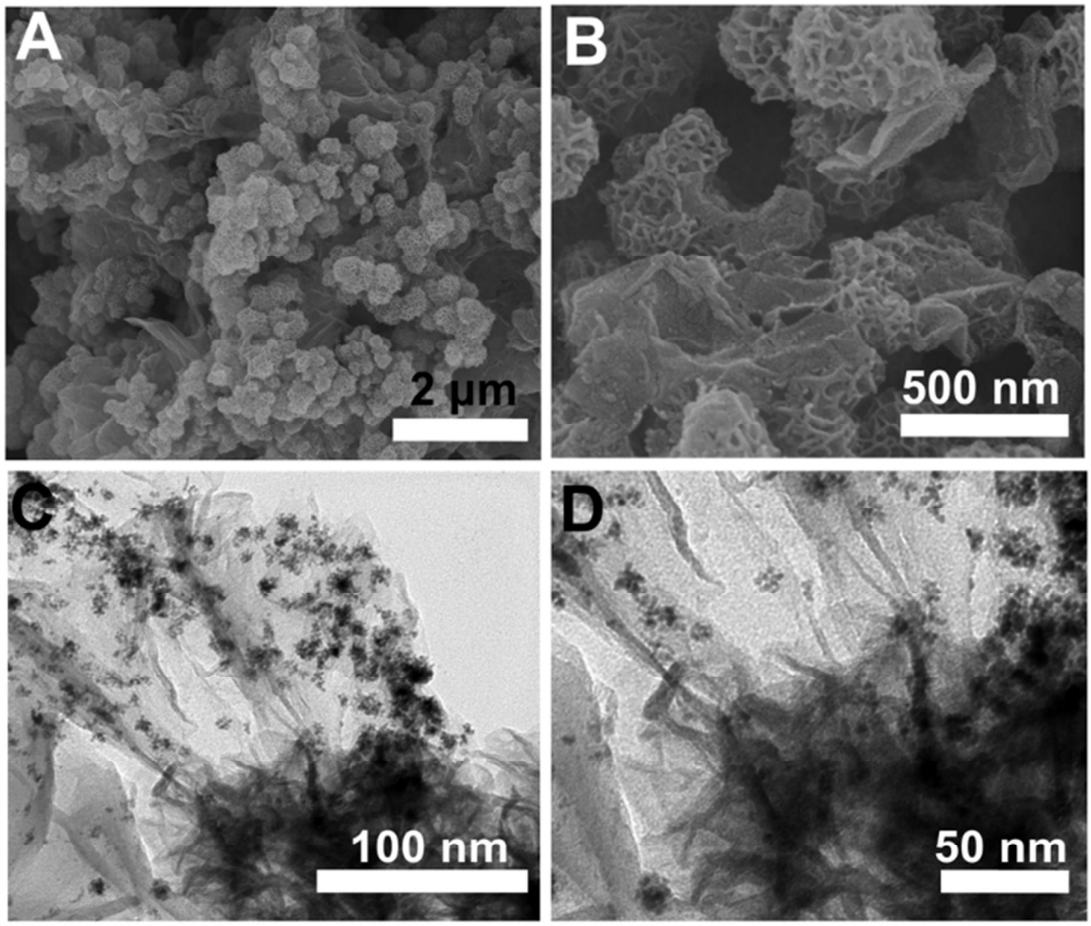

Fig. 3. SEM (A and B) and TEM (C and D) images of 3D Pt/RGO/MnO_2 nanostructures.

The crystal structures of the as-prepared MnO_2, Pt/RGO and Pt/RGO/MnO_2 were further analyzed by XRD, as shown in Fig.4A. In the XRD pattern of MnO_2, the diffraction peaks observed at 12.9°, 25.1°, 37.3° and 65.8° are attributed to (110), (220), (211) and (002) crystal planes of a pure tetragonal the α-MnO_2 phase (JCPDS, file no. 44-0141), suggesting that the crystal of as-synthesized MnO_2 is alpha crystal phase.[21,22] For dendtric Pt/RGO nanostructures, the broad peak at around 24.3° can be assigned to the (002) facet of the crystalline graphite implying that the GO was reduced to RGO.[25] Meanwhile, the diffraction peaks located at about 39.80°, 46.25° and 67.72° which can be indexed to the (111), (200) and (220) reflections of the face-centered cubic (fcc) phase Pt.[13,29] After decorating with MnO_2 and Pt/RGO, 3D tentary Pt/RGO/MnO_2 composite shows all the peaks prepared in the XRD pattern of MnO_2 and Pt/RGO, exhibiting the successful hybridization of the dendritic Pt/RGO nanostructures and α-MnO_2 nanoflowers.

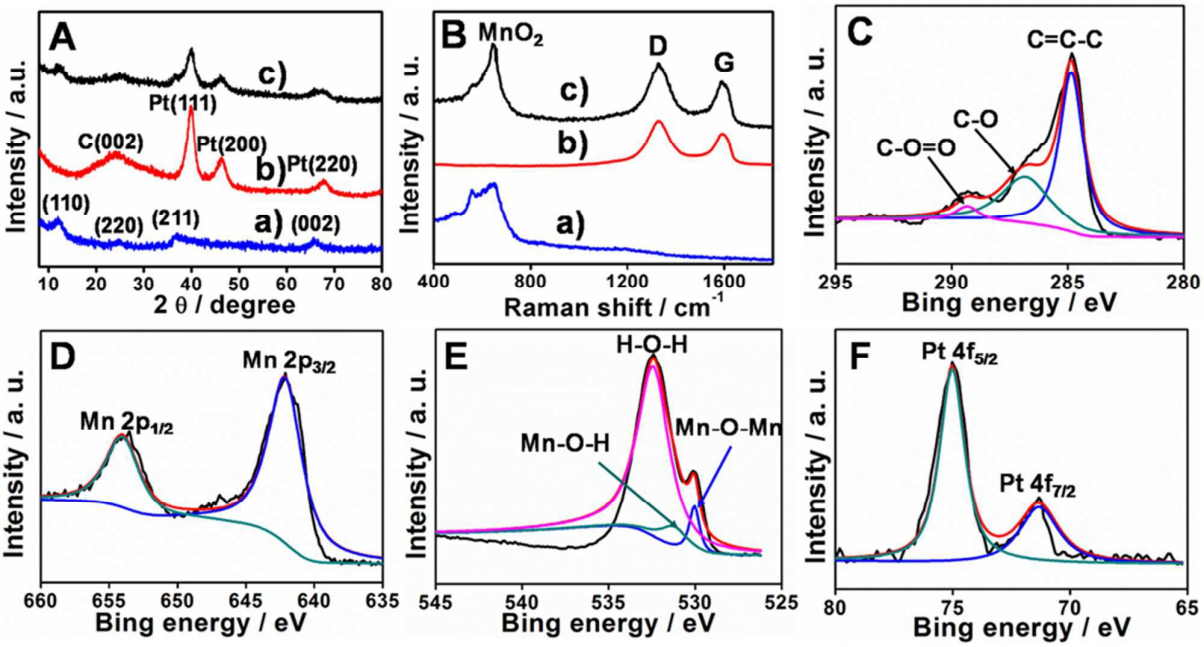

Fig. 4. XRD (A) and Raman spectra (B) of MnO_2 (a), Pt-RGO (b) and Pt/RGO/MnO_2 (c) nanocomposites. XPS spectra of C 1s (C), Mn 2p (D), O 1s (E) and Pt 4f (F) in the Pt/RGO/MnO_2 nanocomposites.

Raman spectroscopy is a noninvasive technique to distinguish ordered and disordered crystal structures of carbonaceous materials. Fig. 4B shows the typical Raman spectra of MnO_2, Pt/RGO and Pt/RGO/MnO_2 composites. For RGO based samples, the results reveal two prominent peaks corresponding to the D and G bands of graphene species are observable at 1329 and 1593 cm^{-1}. The intensity ratio (I_D/I_G) of the D band to G band in Pt/RGO and Pt/RGO/MnO_2 nanocomposites is *ca.* 1.27, which is higher than that of the bare GO sheets (*ca.* 0.81).[30] The increase of I_D/I_G is owing to the reduction and restoration of the sp^2 network in GO.[30,31] This result suggests that the GO was efficiently reduced during the thermal reduction process. In addition, in the Raman spectra of MnO_2 and Pt/RGO/MnO_2, two peaks located at about 555 and 645 cm^{-1} are related to the $\upsilon_{3\ (Mn-O)}$ stretching vibrations and $\upsilon_{2\ (Mn-O)}$ symmetric stretching vibrations of MnO_6 groups, respectively.[32] These results further demonstrate the existence of Pt/RGO and MnO_2 in the as-prepared ternary composite.

XPS is a useful surface chemical analysis technique, which is used to determine the species and chemical states of the elements in the surface of the materials. Fig. 4C~4F shown XPS spectra of C 1s, Mn 2p, O 1s and Pt 4f orbitals of the ternary Pt/RGO/MnO_2 complex. As shown in Fig. 4C, the C 1s XPS spectrum show binding energies at 284.84 eV (C=C-C bonds), 286.82 eV (C-O bonds) and 289.32 eV (O-C=O bonds). The dramatically decrease intensity of oxygen-containing groups C-O bonds and O-C=O bonds, demonstrating that GO was successfully reduced to RGO.[30] As Fig. 4D shown the XPS spectrum of Mn 2p signal consists of two peaks centered at 654.02 eV and 642.12 eV, which can be attributed to the Mn $2p_{1/2}$ and Mn $2p_{3/2}$, respectively. The peaks of Mn $2p_{1/2}$ and Mn $2p_{3/2}$ peak also well agree with those of pure α-MnO_2, further suggesting the formation of alpha crystal phase.[33] Fig. 4E presents the XPS spectrum of O 1s, which reflects the existence of Mn-oxide phases. The spectrum can be deconvoluted into three constituents corresponding to the tetravalent oxide Mn-O-Mn bond (530.02 eV), hydroxide Mn-O-H bond (531.22 eV) and residual water H-O-H bond (532.42 eV).[33] Additionally, the typical spectrum of Pt 4f, the peaks of Pt $4f_{5/2}$ and $4f_{7/2}$ can be observed at 75.02 and 71.32 eV, respectively, indicates that Pt is present in the metallic state, as shown in Fig. 4F.[29]

3.2 Electrocatalytic activity on the modified electrodes

The electrochemical behaviors of the RGO, Pt/RGO, MnO_2 and Pt/RGO/MnO_2 modified electrodes were investigated via cyclic voltammetry (CV) in 10 mM $Fe(CN)_6^{3-/4-}$ and 0.1 M KCl solution at a scan rate of 50 mV s^{-1}. As displayed in Fig. 5A, the 3D ternary Pt/RGO/MnO_2 composite exhibits a tremendously increase peak current (i_{pa}: 152.8 μA) compared to the bare RGO, Pt/RGO, MnO_2 nanostructues. This is attributed to the synergistic effect of dendtric Pt nanostructures, RGO and MnO_2 flower-like sheets. On one hand, the 3D hierarchical nanostructures endow with more surface-to-volume ratio and active sites. On the other hand, the excellent conductivity of RGO sheets might promote the electron transfer between the redox probe and the electrode surface. The electrochemical responses of the four modified electrodes to 0.1 M PBS (pH=7) solution containing 0.5 mM DA are investigated by cycling the potential between −0.20 and +0.60 V (vs. SCE) at 50 mV s^{-1} as depicted in Fig. 5B. Compared to those obtained oxidation current at the MnO_2 (8.76 μA), RGO (18.52 μA) and Pt/RGO (31.01 μA), the Pt/RGO/MnO_2 modifed electrode appears a remarkably larger peak current (78.83 μA). Moreover, it is

noted that the most narrow peak potential difference for Pt/RGO/MnO_2 is 80.3 mV. The increased peak current and decreased peak potential indicate that the Pt/RGO/MnO_2 possess an excellent catalytic activity toward DA sensing compared to that of the RGO, MnO_2 nanoflowers and dendtric Pt/RGO nanostructures.

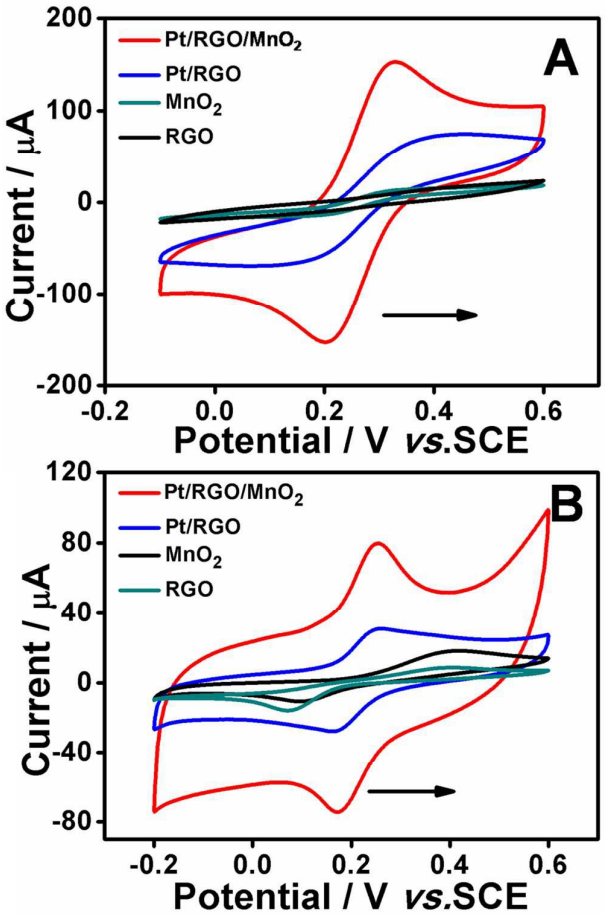

Fig. 5. CVs of Pt/RGO/MnO_2, Pt/RGO, MnO_2, RGO electrodes recorded in 10 mM $Fe(CN)_6^{3-/4-}$ + 0.1 M KCl solution (A), 0.1 M PBS (pH=7.0) containing 0.5 mM DA (B). Scan rate: 50 mV s^{-1}.

3.3 Electrochemical parameters of DA at Pt/RGO/MnO_2 modified electrode

The influence of scan rate on the electrochemical responses of Pt/RGO/MnO_2 is investigated. Fig. 6A shows CVs of 0.1 M PBS (pH=7.0) solution containing 0.5 mM DA at different scan rates ranging from 20 to 200 mV s^{-1}. It can be found that both cathodic and anodic peak currents increase linearly with the scan rate and the calibration equations are I_{pa} (μA) = 0.8436 υ (mV s^{-1}) + 24.0107 (R^2 = 0.998) and I_{pc} (μA) = - 0.8253 υ (mV s^{-1}) – 13.7027 (R^2 = 0.998) (Fig. 6B), suggesting that the electron transfer for DA at ternary Pt/RGO/MnO_2 electrode is an adsorption controlled process. Additionally, it can be seen that the redox peak potentials shifted slightly along with the increase of the scan rate, suggesting a quasi-reversible electrochemical process.[34] The linear regression equations of E_{pa} and E_{pc} versus the logarithm of the scan rates are expressed as E_{pa} = 0.07356 lg υ + 0.1315 (R^2 = 0.992) and E_{pc} = - 0.06721 lg υ + 0.279 (R^2 = 0.993) (Fig. 6C). The electron transfer coefficient (α) and the electron transfer number (n) are calculated according to the following Laviron's equation[34]

$$E_{pa} = E^{0\prime} + 2.30\left(\frac{RT}{(1-\alpha)nF}\right)\lg \upsilon \qquad (1)$$

$$E_{pc} = E^{0\prime} - 2.30\left(\frac{RT}{\alpha nF}\right)\lg \upsilon \qquad (2)$$

where α is the electron transfer coefficient, n is the number of electron transferred, υ is the scan rate and $E^{0\prime}$ is the formal potential. R, T and F have their conventional meanings. According Equ.1 and Equ.2, the α and n are 0.52 and 1.68, respectively, which means there about two electrons are involved in the reaction of DA. This is also consistent with the other reported results.[35,36]

The solution pH is an important factor which influences the electrochemical reaction. Fig. 6D display the CVs of 0.1 M PBS solutions containing 0.5 mM DA with the pH ranging from 5.0 to 8.0. It can be observed that the largest anodic peak current is obtained at the pH of 6.0. According to the human physiological condition (pH 7.0), thus 0.1 M PBS solution with pH=7.0 is chosen for determination of DA. The redox peak of DA shifts negatively along with the increasing pH, which is a consequence of protons involved the redox reactions.[36] The linear relationship between the anodic peak potential (E_{pa}) and pH with slope of 76.86 mV/pH is observed (Fig. 6E), which is close to the anticipated Nernstian value of 59 mV pH^{-1} at 25 °C,[37] indicating that the electron transfer is accompanied by an equal number of protons in electrode reaction. Thus, for the oxidation of DA two electrons and two protons are involved, shown as follows:[2,5]

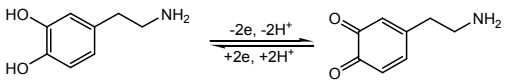

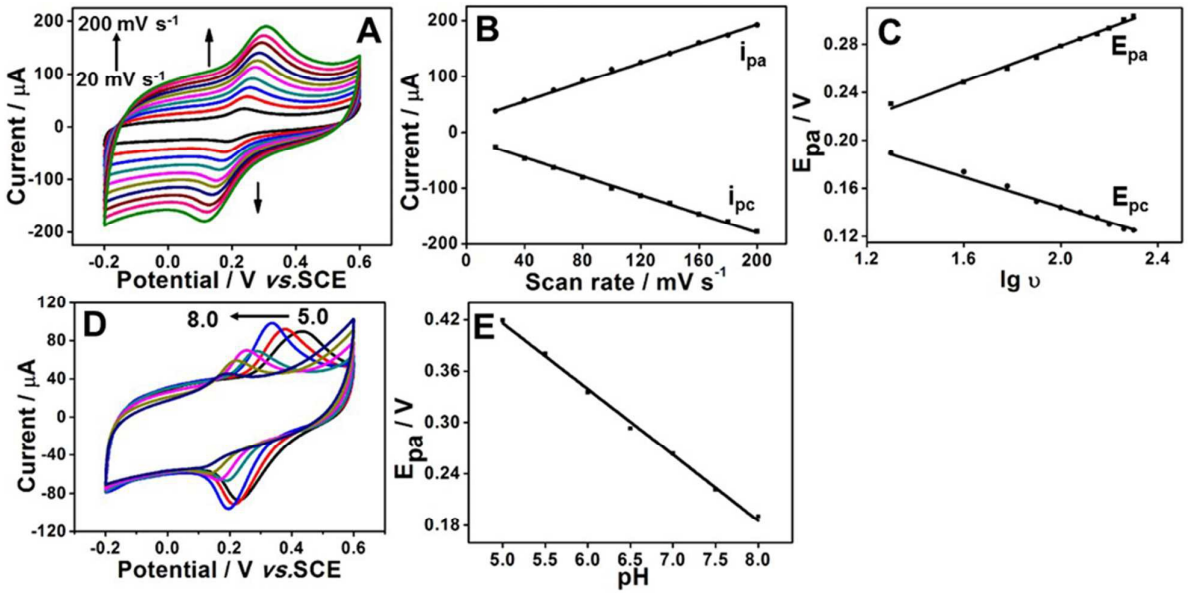

Fig. 6. CVs of the Pt/RGO/MnO_2 electrode in 0.1 M PBS (pH=7.0) solution containing 0.5 mM DA at scan rates from 20 to 200 mV s^{-1} (A), 0.1 M PBS solutions containing 0.5 mM DA with the pH ranging from 5.0 to 8.0 (D) . The plots of anodic and cathodic peak currents to the scan rates (B), anodic and cathodic peak potentials versus lg υ (C), anodic peak potential against pH (E).

3.4 Determination of DA on the Pt/RGO/MnO_2 modified electrode

Differential pulse voltammetry (DPV) commonly has the higher sensitivity than the CV technology, accordingly, the DPV technology is applied for the quantitative detection of DA via the as-prepared Pt/RGO/MnO_2 modified electrode. Fig.7A and 7B depict the DPV curves at Pt/RGO/MnO_2 electrode in 0.1 M PBS (pH=7.0) containing various DA concentrations. It can be observed that the oxidation peak current exhibits remarkable enhancement with the increase of DA concentration. The oxidation peak current of DA versus its concentration at the modified electrode has a good linearity in the range 1.5-215.56 μM with two linear functions I_{pa} (DA) = 1.9162 C – 0.0726, R^2 = 0.992 (C_{DA} = 1.5-26.07 μM) and I_{pa} (DA) = 0.2212 C + 56.0636, R^2 = 0.997 (C_{DA} = 26.07-215.56 μM). The detection limit (LOD) is found to be 0.1 μM (S/N = 3) with a high sensitivity of 1916.2 μA mM^{-1}, which is lower than those modified electrodes listed in Table S1.

3.5 Effect of AA and UA on the detection of DA

As known, the DA, UA and AA molecules are always coexisted in human metabolism. Since the electrochemical property of UA and AA are similar to DA, UA and AA have become the major interferences in the detection of DA. Fig. S2 shows the DPV curves of mixture solution of 5 mM AA, 0.05 mM DA and 0.05 mM UA at Pt/RGO/MnO_2, Pt/RGO, MnO_2, RGO modified GCE electrodes. It can be seen that only small broad and overlapped oxidation peaks of AA, DA and UA were observed at Pt/RGO, MnO_2, RGO modified electrodes. However, three well defined oxidation peaks were easily detected on the Pt/RGO/MnO_2 electrode, which suggest no interference for the selective determination of DA in the presence of AA and UA. To further confirm the selectivity of the Pt/RGO/MnO_2 electrode, the cyclic voltammogram (CV) also are recorded for the three mixture solution, as shown in Fig S3. Three characteristic peaks for AA, DA and UA are clearly observed. The DPV curves at Pt/RGO/MnO_2 electrode in 0.1 M PBS (pH 7.0) containing 5 mM AA, 0.1 mM UA and different concentrations of DA are shown in Fig. 7C and Fig. 7D. It is found that the oxidation peak currents of DA in the presence of AA and UA is increased linearly with the concentrations of DA in the range of 1.5-290.03 μM. The linear regression equation are calibrated as I_{pa} (DA) = 0.7112 C + 39.4606, R^2 = 0.996 (C_{DA} = 1.5-19.92 μM) and I_{pa} (DA) = 0.1427 C + 83.4258, R^2 = 0.995 (C_{DA} = 19.92-290.03 μM) with a lower detection limit of 0.1 μM. This result indicates that DA can still be selectively detected by the 3D ternary Pt/RGO/MnO_2 composite modified electrode in the presence of high concentration of AA and UA.

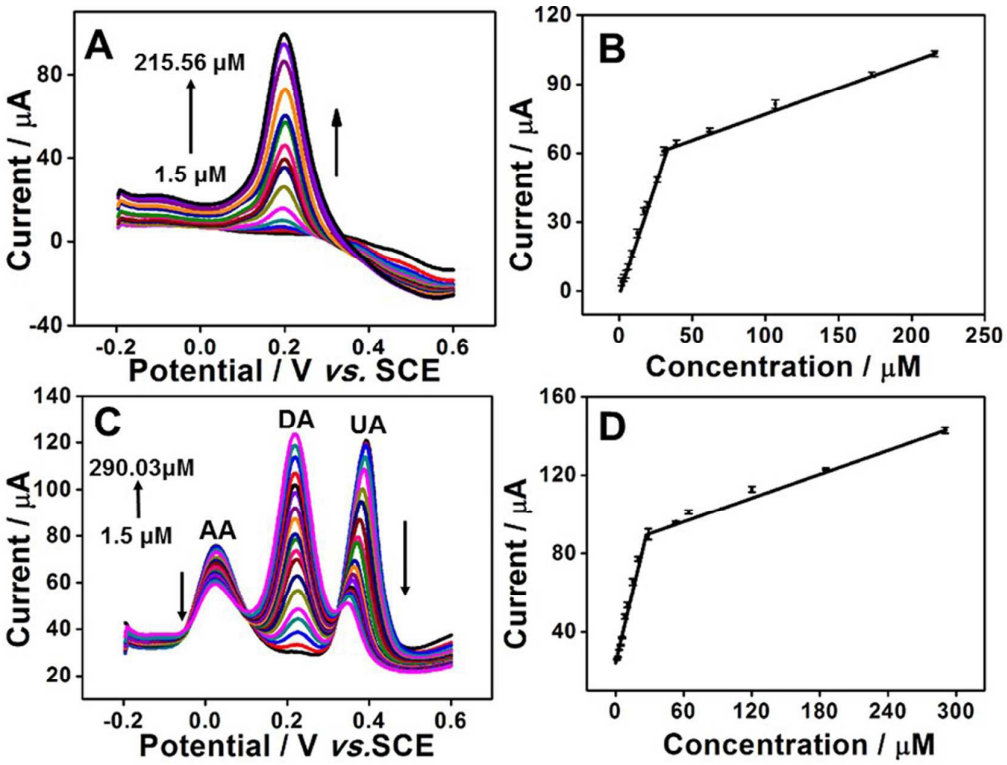

Fig.7. DPV curves of the Pt/RGO/MnO_2 electrode in 0.1 M PBS (pH=7.0) solution containing different concentrations of DA from 1.5-215.56 μM (A), 5 mM AA and 0.1 mM UA with different concentrations of DA from 1.5-290.03 μM (C). (B) and (D): Plots of oxidation currents versus the concentration of DA for consponding spectra of (A) and (C), respectively.

3.6 Repeatability, stability, interference and real sample analysis on the Pt/RGO/MnO_2 modified electrode

Repeatability, stability and interference are key elements of electrode performance. Five parallel 3D Pt/RGO/MnO_2 composite modified electrodes are used to investigate their current responses to 0.5 mM DA in 0.1 M PBS (pH 7.0). The relative standard deviation (RSD) is found to be 2.6%, confirming that the as-prepared Pt/RGO/MnO_2 electrode has a high repeatability. Fig. 8A depicts that the oxidation current response of the sensor still remains up to 96.03% of the initial values after 100 successive assays, indicating that the prepared electrode has a good stability. When the prepared electrode is stored at room temperature and a test performed every 10 days. As shown in Fig. 8B, the response current of the electrode has no obvious signal change compared to its initial response after 50 days, suggesting that the as-synthesized electrode present excellent storage stability. Furthermore, the interference from coexisting species of DA is also investigated, as shown in Fig. 8C. Beside the DA molecule, the 100-fold concentrationof NaCl and KCl, 10-fold concentration of AA, UA and glucose are chosen as the interferential species in the tests. The relative errors are 0%, 1.53%, -3.94%, -5.97%, 0.56%, respectively. This result futher indicates that the as-synthesized 3D Pt/RGO/MnO_2 modified electrode displays well anti-interference ability for the determination of DA. To illustrate the feasibility and application potential of the electrode, Pt/RGO/MnO_2 composite was applied to determine rat serum using the standard addition technique. All samples were diluted with 0.1 M PBS (pH 7.0) and transferred to the electrochemical cell before the measurements. Certain amounts of DA were added into the above mentioned diluted samples, in order to ascertain the correctness of the results. The assay results were also compared with reference values tests (provided by Second Affiliated Hospital of Suzhou University) listing in Table S2 with the relative errors ranged from -8.41% to 5.7%. It was obviously found that Pt/RGO/MnO_2 exhibited exact effectively used for determination of DA in real samples.

4. Conclusions

In summary, an electrochemical sensor for highly sensitive and selective determination of DA is synthesized including 3D dendritic Pt/RGO and MnO_2 nanoflowers. The electrocatalytic analysis results indicated that the 3D ternary Pt/RGO/MnO_2 composite has apparently enhanced electrochemical performance for the detection of DA compared with bare RGO, dendritic Pt/RGO, MnO_2 nanoflowers modified electrodes. The higher electrocatalytic performance is owing to the synergistic effect of dendtric Pt nanostructures, RGO and MnO_2 flower-like sheets, where an extraordinarily fast electron transfer rate for the oxidation of DA on the ternary composite modified electrode surface. Moreover, the ternary proposed electrode also displays selective, sensitive determination of DA with well

repeatability and anti-interference in the presence of large excess of AA and UA. These features reveal that the 3D hierarchical ternary Pt/RGO/MnO_2 composite can be used as a promising highly sensitive and selective electrochemical sensor with excellent reproducibility and anti-interference in the future.

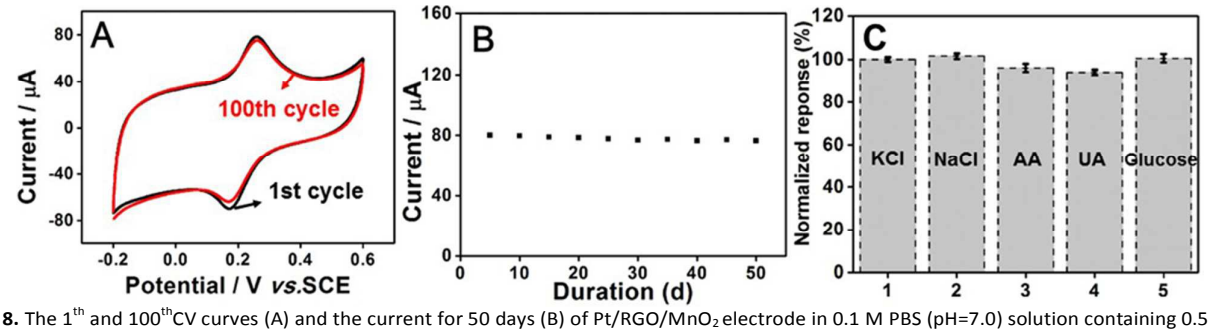

Fig. 8. The 1th and 100thCV curves (A) and the current for 50 days (B) of Pt/RGO/MnO_2 electrode in 0.1 M PBS (pH=7.0) solution containing 0.5 mM DA at scan rate of 50 mV s^{-1}. (C) Results of interference study on the response of 100-fold KCl and NaCl, 10-fold AA, UA and glucose.

Acknowledgment

This work was supported by the NSFC (51373111), Suzhou Nano-project (ZXG2012022), the Project of Scientific and Technologic Infrastructure of Suzhou (SZS201207), the Academic Award for Young Graduate Scholar of Soochow University and the Priority Academic Program Development of Jiangsu Higher Education Institutions (PAPD).

Notes and references

[a] College of Chemistry, Chemical Engineering and Materials Science, Soochow University, Suzhou 215123, P.R. China.
E-mail: duyk@suda.edu.cn; Fax: +8651265880089; Tel: +86 512 65880361
[b] Department Chemistry, University of Toronto, Toronto M5S 3H6, Canada
E-mail: mingshanzhu@yahoo.com

1. M. Zhang, C. Liao, Y. Yao, Z. Liu, F. Gong, F. Yan, *Adv. Funct. Mater.*, 2014, **24**, 978.
2. G. She, X. Huang, L. Jin, X. Qi, L. Mu, W. Shi, *Small*, 2014, **10**, 4685.
3. K. Jackowska, P.Krysinski, *Anal Bioanal Chem.*, 2013, **405**, 3753.
4. J. Du, R. Yue, F. Ren, Z. Yao, F. Jiang, P. Yang, Y. Du, *Biosens. Bioelectron.*, 2014, **53**, 220.
5. J. Salamon, Y. Sathishkumar, K. Ramachandran, Y. Lee, D. Yoo, A. Kim, G. Gnanakumar, *Biosens. Bioelectron.*, 2015, **64**, 269.
6. F. Wang, S. Hu, *Microchim. Acta*, 2009, **165**, 1.
7. S. Mahshid, C. Li, S. Mahshid, M. Askari, A. Dolati, L. Yang, S. Luo, Q. Cai, *Analyst*, 2011, **136**, 2322.
8. S. S. JyothirmayeeAravind, S. Ramaprabhu, *Sens. Actuators, B*, 2011, **155**, 679.
9. X. Yu, Y. Zhang, L. Guo, L. Wang, *Nanoscale*, 2014, **6**, 4806.
10. L. Wang, Y. Yamauch, *J. Am. Chem. Soc.*, 2009, **131**, 9152.
11. M. A. Mahmoud, C. E. Tabor, M. A. El-Sayed, Y. Ding, Z. Wang, *J. Am. Chem. Soc.*, 2008, **130**, 4590.
12. L. Ma, C. Wang, M. Gong, L. Liao, R. Long, J. Wang, D. Wu, W. Zhong, M. J. Kim, Y. Chen, Y. Xie, Y. Xiong, *ACS Nano*, 2012, **6**, 9797.
13. G. How, A. Pandikumar, H. Ming, L. Ngee, *Sci. Rep.*, 2014, **4**, 5044.
14. A. Pandikumar, G. How, T. See, F. Omar, S. Jayabal, K. Kamali, N. Yusoff, A. Jamil, R. Ramaraj, S. John, H. Lim, N. Huang, *RSC Adv.*, 2014, **4**, 63296.
15. S. Guo, S. Dong, E. Wang, *ACS Nano*, 2010, **4**, 547.
16. M. Zhu, B. Lei, F. Ren, P. Chen, Y. Shen, B. Guan, Y. Du, T. Li, M. Liu, *Sci. Rep.*, 2014, **4**, 1.
17. M. Zhou, Y. Zhai, S. Dong, *Anal. Chem.,* 2009, **81**, 5603.
18. C. Chung, Y. K. Kim, D. Shin, S. R. Ryoo, B. H. Hong, D. H. Min, *Accounts Chem. Res.,* 2013, **46**, 2211.
19. S. Chen, J. Zhu, X. Wu, Q. Han, X. Wang, *ACS Nano*, 2010, **4**, 2822.
20. Z. Wu, W. Ren, D. Wang, F. Li, B. Liu, H. Cheng, *ACS Nano*, 2010, **4**, 5835.
21. K. Dai, L. Lu, C. Liang, J. Dai, Q. Liu, Y. Zhang, G. Zhu, Z. Liu, *Electrochim. Acta*, 2014, **116**, 111.
22. H. Zhao, Y. Dong, P. Jiang, G. Wang, J. Zhang, K. Li, C. Feng, *New J. Chem.*, 2014, **38**, 1743.
23. Y. Huang, C. Cheng, X. Tian, B. Zheng, Y. Li, H. Yuan, D. Xiao, M. M. F. Choi, *Electrochim. Acta*, 2013, **89**, 832.
24. T. Gan, J. Sun, K. Huang, L. Song, Y. Li, *Sens. Actuators, B*, 2013, **177**, 412.
25. R. Liu, H. Zhou, J. Liu, Y. Yao, Z. Huang, C. Fu, Y. Kuang, *Electrochem. Commun.*, 2013, **26**, 63.
26. F. Ren, H. Wang, C. Zhai, M. Zhu, R. Yue, Y. Du, P. Yang, J. Xu, W. Lu, *ACS Appl. Mater. Interfaces*, 2014, **6**, 3607.
27. W. Xu, S. Xue, H. Yi, P. Jing , Y. Chai, R. Yuan, *Chem. Commun.,* 2015, **51**, 1472.
28. Y. Zhang, M. Su, L. Ge, S. Ge, J. Yu, X. Song, *Carbon,* 2013, **57**, 22.
29. M. Zhu, Y. Du, P. Yang, X. Wang, *Catal. Sci. Technol.*, 2013, **3**, 2295.
30. C. Zhai, M. Zhu, Y. Lu, F. Ren, C. Wang, Y. Du, P. Yang, *Phys. Chem. Chem. Phys.*, 2014, **16**, 14800.
31. Z. Yao, M. Zhu, F. Jiang, Y. Du, C. Wang, P. Yang, *J. Mater. Chem.*, 2012, **22**, 13707.
32. X. Xie, L. Gao, *Carbon*, 2007, **45**, 2365.
33. H. Cheng, L. Long, D. Shu, J. Wu, Y. Gong, C. He, Z. Kang, X. Zou, *Int. J. Hydrogen Energy*, 2014, **39**, 16151.
34. W. Sun, L. Cao, Y. Deng, S. Gong, F. Shi, G. Li, Z. Sun, *Anal. Chim. Acta*, 2013, **781**, 41.
35. A. Yang, Y. Xue, Y. Zhang , X. Zhang, H. Zhao, X. Li, Y. He, Z. Yuan, *J. Mater. Chem. B*, 2013, **1**, 1804.
36. G. Liu, H. Chen, G. Lin, P. Ye, X. Wang, Y. Jiao, X. Guo, Y. Wen, H. Yang, *Biosens. Bioelectron.*, 2014, **26**, 56.
37. C. Lim, H. Hoh, P. Ang, K. Loh, *Anal. Chem.,* 2010, **82**, 7387.

Table of Content

A highly sensitive and selective electrochemical sensor: 3D hierarchical ternary composite including Pt nanodendrites/reduce graphene oxide/MnO_2 nanoflowers modified electrode.